

VORONOÏ REGION-BASED ADAPTIVE UNSUPERVISED COLOR IMAGE SEGMENTATION

R. HETTIARACHCHI^α AND J.F. PETERS^{α,β}

ABSTRACT. Color image segmentation is a crucial step in many computer vision and pattern recognition applications. This article introduces an adaptive and unsupervised clustering approach based on Voronoï regions, which can be applied to solve the color image segmentation problem. The proposed method performs region splitting and merging within Voronoï regions of the Dirichlet Tessellated image (also called a Voronoï diagram), which improves the efficiency and the accuracy of the number of clusters and cluster centroids estimation process. Furthermore, the proposed method uses cluster centroid proximity to merge proximal clusters in order to find the final number of clusters and cluster centroids. In contrast to the existing adaptive unsupervised cluster-based image segmentation algorithms, the proposed method uses K-means clustering algorithm in place of the Fuzzy C-means algorithm to find the final segmented image. The proposed method was evaluated on three different unsupervised image segmentation evaluation benchmarks and its results were compared with two other adaptive unsupervised cluster-based image segmentation algorithms. The experimental results reported in this article confirm that the proposed method outperforms the existing algorithms in terms of the quality of image segmentation results. Also, the proposed method results in the lowest average execution time per image compared to the existing methods reported in this article.

1. INTRODUCTION

Image segmentation plays a major role in many computer vision and pattern recognition applications. According to [6], image segmentation is the process of dividing an image into different regions such that each region is, but the union of any two adjacent regions is not, homogenous. The existing image segmentation techniques can be broadly categorized into threshold-based, clustering-based, region-based, edge-based and physics-based segmentation approaches [17, 6]. There are various hybrid image segmentation techniques, which combine two or more of the aforementioned approaches. Clustering techniques have been widely used to cluster image pixels based on the similarity of their features (e.g. color, texture, etc.). K-means [14] and Fuzzy C-means (FCM) [4] are two of the most popular clustering techniques used for image segmentation.

Clustering is an unsupervised learning process, which does not require class labeled data set as training data to cluster unknown set of data into clusters. According to [16], a cluster is comprised of a number of similar objects (pixels in our case) collected or grouped together. In traditional clustering techniques such as K-means and FCM, the number of clusters has to be predefined to initiate the algorithm.

Key words and phrases. Voronoï Regions, Adaptive Unsupervised Clustering, Image Segmentation.

Also, the initial cluster centers (or centroids) are not known. For example, the K-means algorithm starts with random cluster centers initially as starting points and then iteratively adjusts the centroids until the algorithm converges. This process is time consuming and may not produce the intended result.

In contrast to K-means, FCM returns the membership weights for each point in the data set, which define the degree of belonging of a data point to a given cluster. A given data point will have a high membership weight (higher degree of belonging) to a nearby cluster a low membership weight for a faraway cluster. [12] claims that K-means is faster and better compared to FCM algorithm.

In the case of color images, which are complex data sets by nature, the determination of the number of pixel clusters and the cluster centroids becomes very challenging. Thus, adaptive unsupervised clustering techniques, which automatically find the number of clusters and the corresponding cluster centroids is vital for successful image segmentation via clustering techniques. Due to this reason, during the recent past, the focus of many researchers has turned towards adaptive unsupervised clustering techniques for image segmentation. Mean-Shift algorithm introduced by Fukunaga and Hostetler [11] is a non-parametric clustering algorithm, which does not require the number of clusters to be predefined. However, Mean-Shift is very much slower compared to K-means algorithm. The time complexity of classical K-means is $O(knT)$ while the time complexity of Mean-Shift is $O(Tn^2)$.

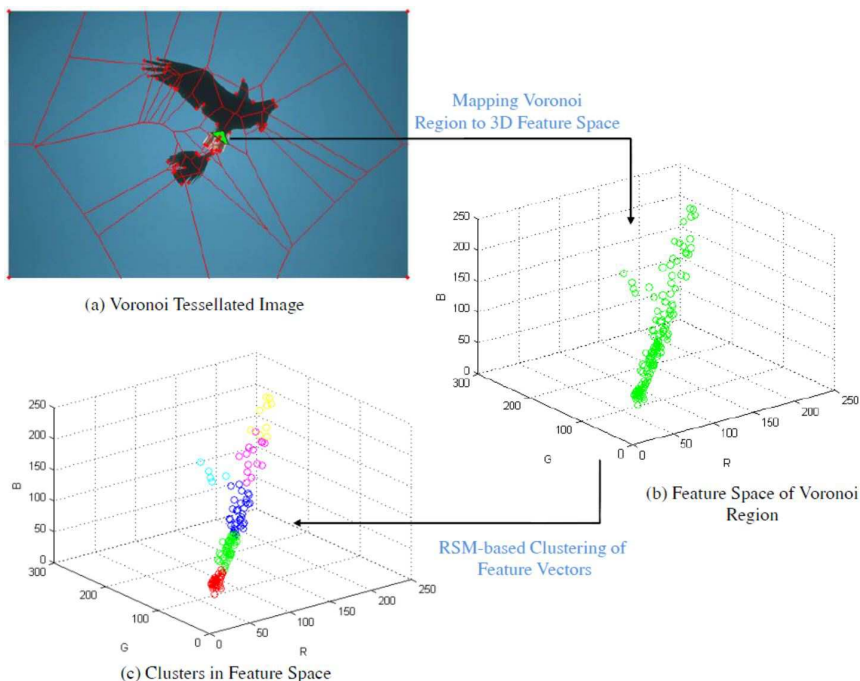


FIGURE 1. Intra-Voronoi region clustering

Recently, Yu et al. in [38] proposed an adaptive unsupervised algorithm called Ant ColonyFuzzy C-means Hybrid Algorithm (AFHA), which is a combination of

Ant System and Fuzzy C-mean techniques. In [38], Ant System (AS) [7] is used to determine the number of clusters and the cluster centroids. It is said in [38] that AFHA outperforms other state-of-the-art segmentation technique, such as X-means [24], Mean-Shift, Normalized Cut [31]. Another unsupervised adaptive clustering approach for image segmentation named Region Splitting and Merging-Fuzzy C-means Hybrid Algorithm (RFHA) is proposed in [34] by Tan et al. RFHA algorithm uses region splitting and merging scheme to determine the number of clusters and cluster centroids. Both of these algorithms use Fuzzy C-means algorithm to find the final segmented image. Some other adaptive clustering approaches for image segmentation can be found in [36, 33, 30, 15, 35, 2].

The computational complexity of the AFHA algorithm is very high due to the complicated nature of the AS module that it uses. Thus Yu et al. proposed a modified version of AFHA algorithm named improved AFHA (IAFHA) in [38], which finds the number of clusters and cluster centroids via AS by taking only a small proportion (about 30%) of the total number of pixels into account. This modification in IAFHA significantly reduces the computational complexity of the original AFHA algorithm, but it affects the performance of the algorithm at the same time. RFHA is faster compared to AFHA. However, both of these algorithms suffer from the high computational complexity of the FCM algorithm.

In this article, we propose a Voronoï region-based adaptive unsupervised algorithm to automatically find the number of clusters and the cluster centroids in a given set of pixels. First, the proposed algorithm adaptively divides the image into Voronoï regions and then automatically finds the number of clusters and cluster centroids of the pixels belonging to each of these Voronoï regions by using a region splitting and merging scheme similar to the one given in [34, §2.1] (see figure 1). Next, the intra-Voronoï region clusters that are near each other will be merged together to find the final number of clusters and cluster centroids in a given image. Finally, the final segmented image will be found by applying K-means clustering algorithm on the whole image initiated with the number of clusters and cluster centroids found in the previous step.

The Voronoï region wise clustering in the proposed algorithm reduces the complexity of the segmentation problem significantly, which will be discussed in detail in section 3.2. Furthermore, since the number of possible clusters within a single Voronoï region is usually lower compared to the number of clusters in the whole image, estimating the number of clusters and cluster centroids becomes more efficient and precise.

The rest of the article is organized as follows. Section 2 presents the work related to the method proposed in this article. The methodology of the proposed Voronoï region-based adaptive unsupervised algorithm is presented in section 3. Section 4 discusses the results of experiments conducted on the proposed method and two other adaptive unsupervised cluster-based image segmentation algorithms. Finally, section 5 concludes the research work presented in this article.

2. RELATED WORK

2.1. Image Segmentation. A formal definition of image segmentation given in [23] is as follows.

Definition 1. *Image Segmentation*^[23]

If F is the set of all pixels and $P()$ is a uniformity (homogeneity) predicate defined

on group of connected pixels, then segmentation is a partitioning of the set F into a set of connected subsets of regions (S_1, S_2, \dots, S_n) such that

$$\bigcup_{i=1}^n S_i = F \text{ with } S_i \cap S_j = \emptyset, i \neq j$$

The uniformity predicate $P(S_i) = true$ for all regions (S_i) and $P(S_i \cap S_j) = false$, when S_i is adjacent to S_j . Based on this definition, a segmented image can be evaluated by measuring the homogeneity within each segment and by measuring the overlap between each pair of segments. Haralick et al. proposed four criteria to define a good image segmentation in [13] as follows.

- (1) Regions should be uniform and homogeneous with respect to some characteristic(s).
- (2) Adjacent regions should have significant differences with respect to the characteristic on which they are uniform.
- (3) Region interiors should be simple and without holes.
- (4) Boundaries should be simple, not ragged, and be spatially accurate.

The first two criteria can be directly derived from the definition 1. Most of the segmentation evaluation methods are based on the first two criteria defined by Haralick et al. [13] given in section 2.1, jointly called the characteristic criteria. The first criterion measures the intra-region uniformity while the second criterion measures the inter-region disparity. Zhang et al. [39] provides a good summary of unsupervised evaluation methods, which fall under both of these categories.

2.2. Dirichlet Tessellation (Voronoi Diagram). Image tessellation is a tiling of an image surface with regular polygons and Dirichlet tessellation (also called Voronoi diagram) is one example of image tessellation. Dirichlet [8] introduced polygon-based tessellation in 1850, which was elaborated by Voronoi in 1907 [37]. A Voronoi diagram is the partitioning of a plane with n points into convex polygons such that each polygon contains exactly one generating point and every point in a given polygon is closer to its generating point than to any other. Thus, a Voronoi region can be defined by the following definition,

Definition 2. Voronoi Region

Let S and X be finite sets in a n -dimensional Euclidean space. Let $p \in S$ (denoted V_p) is defined by

$$V_p = \{x \in X : \|x - p\| \leq \forall q \in S \|x - q\|\}.$$

where S is the set of generating points.

Thus, in order to generate the Voronoi diagram, the generating points or the seed points have to be provided. In our context, these seed points can be *corners*, *centroids*, *critical points*, *key points* found in images. For example, Du et al. introduced the technique of Centroidal Voronoi Tessellations (CVT) in 1999 [9], which uses centroids as the generating points for the Voronoi tessellation. In 2006, Du et al. revisits the CVT algorithm in their subsequent article [10], which focus more on the applications of CVT.

Voronoi regions (convex polygons produced by Dirichlet tessellation) have been explored as a solution to the image segmentation problem during the past two decades. An interesting paper on Voronoi based image segmentation is *On Points Geometry for Fast Digital Image Segmentation* [5]. In this paper, rather than applying the Voronoi Diagram on the image itself, it is applied on a few selected

points by using the image histogram. [32] also suggests Voronoï cells for image segmentation. The articles [9, 10] focus on spatial Dirichlet tessellation while [5] focus on Dirichlet tessellation on image histograms.

2.3. Region Splitting and Merging Scheme. A summary of the region splitting and merging scheme proposed in [34, §2.1] is given below.

- (1) Apply the moving average filter with a span of 5 to the histogram of each color channel.
- (2) Identify and remove all the local peaks and valleys in the histogram of each color channel based on the fuzzy rule base given in equation (2) and (3) in [34, §2.1].
- (3) Identify the significant peaks by examining the turning points from positive to negative gradient changes.
- (4) Determine the valleys of each color channel histogram by taking the minimum value between any adjacent peaks.
- (5) Define color cells (classes) based on the combinations of valleys in the histogram of each color channel.
- (6) Assign each pixel to a color cell depending on its color channel values.
- (7) Calculate initial cluster centers by averaging pixels withing a given cell.
- (8) Calculate Manhattan distances between all pairs of cluster centers and find the two nearest clusters.
- (9) Merge the two nearest clusters and update the cluster center.
- (10) Reduce the number of clusters and repeat the process until the shortest distance between two nearest clusters is not less than a predefined threshold.

3. PROPOSED METHOD

As explained in section 2.2, Dirichlet tessellation divides an image into polygonal regions based on the spatial locations (X and Y coordinates) of the seed points (generating points). These polygonal Voronoï regions are much simpler to analyze and process compared to the whole image. Also, since the seed points can be derived from a given image, a tessellation is tailored to the structure of the image itself. Since, these image features are found spatially in an image, we call this process *spatial Dirichlet tessellation*, which divides an image into N number of Voronoï regions, where N is the number of seed points.

$$V = \{V_1, V_2, \dots, V_N\}.$$

Once a Dirichlet tessellation of a given image is found, the next step is to further divide each Voronoï region V_p until the whole image is grouped into small similar regions. Thus, next we consider the feature space of each Voronoï region. If each pixel within a given Voronoï region V_p is represented by its d-dimensional feature vectors, then each pixel in V_p can be mapped to a point on a d-dimensional feature space.

$$(1) \quad V_p \rightarrow X_p, \text{ where } X_p \subset \mathbb{R}^d \text{ and } \Phi : \mathbb{R}^2 \rightarrow \mathbb{R}^d \text{ defined by } \Phi(x) = \{\Phi_1(x), \Phi_2(x), \dots, \Phi_d(x)\} = \bar{x}.$$

where Φ is a set of probe functions representing features of a given pixel x . $\Phi(x) = \bar{x}$ is the feature vector representing the pixel x .

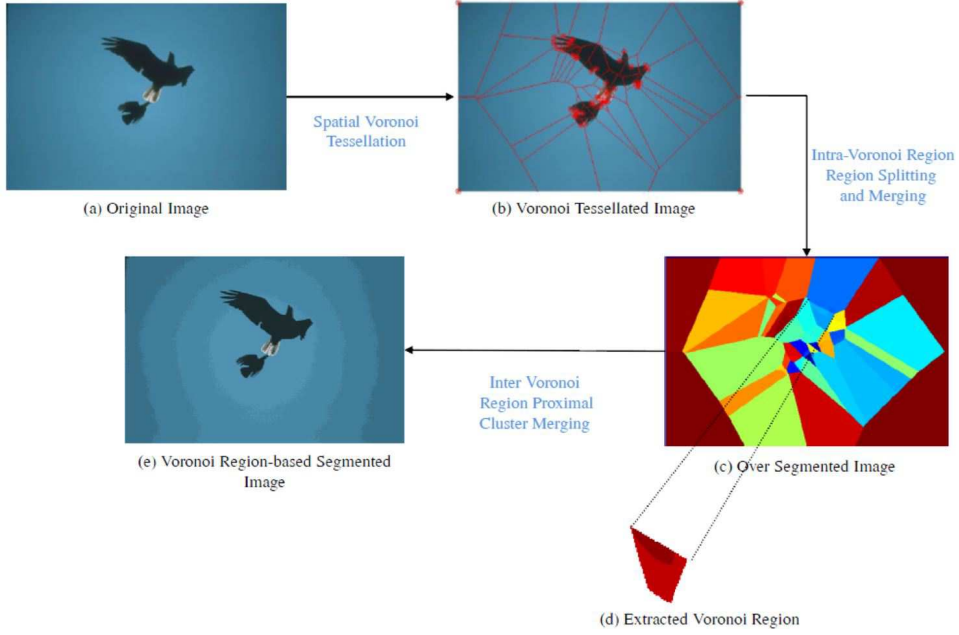


FIGURE 2. Stages of the proposed method

Then, Dirichlet tessellation can be performed on the feature space \mathbb{R}^d , where $d = 3$ in this case as we use R, G and B color channel values of each pixel. For this purpose, the Lloyd style K-means clustering algorithm [22] can be used. K-means clustering partitions the space of observations into k classes such that each observation belongs to the cluster with the nearest mean or the centroid. In an optimal solution, each centroid is assigned the data in its Voronoi region and is located at the center of mass of this data. The Lloyd style K-means clustering algorithm runs iteratively until all the data points in the Voronoi region of a given centroid are clustered together, and then the centroid is moved to the centroid of its cluster [22]. The original Lloyd's algorithm [19], which is also known as Voronoi iteration differs from k-means clustering in that its input is a continuous geometric region rather than a discrete set of points as in K-means clustering.

Once the k-means clustering is performed, the discrete set of points in the feature space fall within the Voronoi regions of the centroids closest to those regions. Therefore, K-means clustering can be used to cluster data into Voronoi regions based on their features. The K-means clustering algorithm requires the number of clusters (k) to be predefined. In the case of the whole image, automatically finding the number of clusters is computationally complex. However, in the case of small Voronoi region, finding the number of clusters will be more effective due to the small number of pixels and small number of clusters within a given Voronoi region. Thus, we propose to use the region splitting and merging (RSM) scheme given in [34] to adaptively determine the number of clusters and cluster centroids for each Voronoi region.

First, the set of pixels within V_p will be mapped into its feature space X_p with the help of equation (1). Then, region splitting and merging will be applied on

X_p in order to find the adaptive feature space Dirichlet tessellation. Let k_p be the number of clusters and C_p be the cluster centroids found by applying RSM on the set of pixel feature points X_p within a given Voronoï region V_p , then X_p can be represented as a set of clusters as given below. Figure 1 depicts the process of intra-Voronoï region clustering.

$$X_p = \{s_1, s_2, \dots, s_{k_p}\}.$$

Once, the feature space Dirichlet tessellation is completed for all the Voronoï regions in the image, the image can be said to be at an over-segmented state. Let the total set of clusters after the feature space Dirichlet tessellation be $S = \{s_1, s_2, \dots, s_P\}$. Since, the clustering was performed within each Voronoï region, there can be clusters with similar features belonging to two different Voronoï regions. Thus, in the next step we find such similar clusters and merge them together to find the final number of clusters and cluster centroids.

In the proposed method, the concept of nearness (proximity) ([25, §1.19], [26, §1.4] and [27]) will be used to find clusters, which are very much similar (proximal) to each other. These proximal clusters can be merged together to form a single cluster. We extend the notion of nearness of clusters to nearness of their respective centroids to compare two clusters.

Definition 3. Cluster Centroid

Let s be cluster, then the centroid of the cluster μ can be defined as,

$$\bar{\mu} = \frac{\sum_{\forall \bar{x}_i \in s} \bar{x}_i}{n}$$

where \bar{x}_i are the feature vectors representing the members of s and n is the number of members in s .

The *Centroid* method can be used, when finding inter-Voronoï region proximal clusters. In the centroid method, *the resemblance between two clusters is equal to the resemblance between their centroids* [28, §9.5]. Thus, clusters whose centroids are closest together are merged. The centroid of a merged cluster is a weighted combination of the centroids of the two individual clusters, where the weights are proportional to the sizes of the clusters [21, pp. 373].

Let s_1, s_2 be two clusters and $\bar{\mu}_1, \bar{\mu}_2$ be their cluster centroids respectively. Then the lemma 1 can be derived for the Centroid method,

Lemma 1. *Let s_i, s_j be two clusters in S and $\bar{\mu}_i, \bar{\mu}_j$ be their cluster centroids respectively. Then,*

$$proximity(s_i, s_j) = proximity(\bar{\mu}_i, \bar{\mu}_j).$$

Proof.

$$\begin{aligned} proximity(\bar{\mu}_i, \bar{\mu}_j) &= \bar{\mu}_i \cdot \bar{\mu}_j \\ &= \left(\frac{1}{n_i} \sum_{\bar{x}_i \in s_i} \bar{x}_i \right) \cdot \left(\frac{1}{n_j} \sum_{\bar{x}_j \in s_j} \bar{x}_j \right) \\ &= \frac{1}{n_i n_j} \sum_{\bar{x}_i \in s_i} \sum_{\bar{x}_j \in s_j} \bar{x}_i \cdot \bar{x}_j \\ &= proximity(s_i, s_j) \end{aligned}$$

□

In the context of this article, the centroid proximity will be defined as,

Definition 4. Centroid Proximity

Let s_i, s_j be two clusters in S and $\overline{\mu}_i, \overline{\mu}_j$ be their cluster centroids respectively. The centroid proximity between $\overline{\mu}_i$ and $\overline{\mu}_j$ will be defined as,

$$\text{proximity}(\overline{\mu}_i, \overline{\mu}_j) = d(\overline{\mu}_i, \overline{\mu}_j)$$

where, $d(\overline{\mu}_i, \overline{\mu}_j)$ is the Manhattan distance (proximity measure) between the two centroids $\overline{\mu}_i$ and $\overline{\mu}_j$ given by,

$$d(\overline{\mu}_i, \overline{\mu}_j) = \sum_{i=1}^n |\Phi_i(\mu_i) - \Phi_i(\mu_j)|.$$

Theorem 1. Let s_i, s_j be two clusters in S and μ_i, μ_j be their cluster centroids respectively.

$$\text{If } d(\overline{\mu}_i, \overline{\mu}_j) < \varepsilon, \text{ then } s_i \delta_d s_j$$

where d is the Manhattan distance metric leading to metric proximity δ_d and ε is a predefined threshold.

Proof. From lemma 1 and definition 4, $\text{proximity}(s_i, s_j) = \text{proximity}(\overline{\mu}_i, \overline{\mu}_j) = d(\overline{\mu}_i, \overline{\mu}_j)$. Thus, if $d(\overline{\mu}_i, \overline{\mu}_j) < \varepsilon$, then $\overline{\mu}_i \delta_d \overline{\mu}_j \Rightarrow s_i \delta_d s_j$. \square

Definition 5. Proximal Clusters

Let s_i, s_j be two clusters in S and $\overline{\mu}_i, \overline{\mu}_j$ be their cluster centroids respectively. The clusters s_i and s_j are called proximal clusters (denoted by $s_i \delta_d s_j$) if, $d(\overline{\mu}_i, \overline{\mu}_j) < \varepsilon$, where ε is a predefined threshold.

Thus, two clusters s_i, s_j can be merged if $d(\overline{\mu}_i, \overline{\mu}_j) < \varepsilon$ and the centroid of the merged cluster can be calculated by using equation (2),

$$(2) \quad \overline{\mu} = \frac{n_i}{n_i + n_j} \overline{\mu}_i + \frac{n_j}{n_i + n_j} \overline{\mu}_j.$$

where n_i and n_j are the number of elements in s_i and s_j respectively.

In the proposed method, the following merge condition derived based on theorem 1 will be used to iteratively merge proximal clusters belonging to different Voronoï regions.

Merge Condition : Let s_i, s_j be two clusters in S such that $s_i \subset X_i, s_j \subset X_j$, where $V_i \rightarrow X_i$ and $V_j \rightarrow X_j, V_i \neq V_j$. s_i and s_j will be merged if $s_i \delta_d s_j$.

All proximal clusters, which satisfy the above merge condition will be found and merged together iteratively until the number of proximal clusters becomes zero. This process yields the final number of clusters k and the cluster centroids C . Finally, K-means clustering on the feature vectors of the total set of pixels $X = \bigcup_{p=1}^N X_p$ of the image will be performed initiated with k and C to find the final segmented image.

3.1. Implementation of the Proposed Algorithm. In the implementation of the proposed algorithm, corner points of an image will be used as generating points of the spatial Voronoï tessellation. The proposed algorithm consists of the following major steps:

- (1) Find the (X,Y) coordinates of the set of the most prominent corners in the image I .
- (2) Generate the Voronoï diagram $V = \{V_1, V_2, \dots, V_N\}$ by taking the set of corner points found in step 1 as the generating points.

- (3) Within each Voronoi region V_p ,
 - (a) Apply RSM on the feature vector set X_p of each Voronoi region V_p to find the number of clusters k_p , cluster centroids C_p and the set of clusters $X_p = \{s_1, s_2, \dots, s_{k_p}\}$.
 - (b) Let the total set of clusters belonging to all Voronoi regions be $S = \{s_1, s_2, \dots, s_P\}$.
- (4) Iteratively merge the inter Voronoi region proximal clusters until the number of proximal clusters become zero.
 - (a) Find pair of clusters $s_i, s_j \in S$, which satisfy the merge condition and $d(\overline{\mu}_i, \overline{\mu}_j) = \inf_{s_x, s_y \in S} (d(\overline{\mu}_x, \overline{\mu}_y))$. where $\overline{\mu}_i$ and $\overline{\mu}_j$ are the centroids of clusters s_i and s_j respectively.
 - (b) Merge s_i and s_j together so that $s_k = s_i \cup s_j$.
 - (c) Find new cluster centroid μ_k of cluster s_k using the equation (2).
 - (d) Update the total number of clusters $P = P - 1$.
 - (e) Repeat steps 4.(a) to 4.(d) until $d(\overline{\mu}_i, \overline{\mu}_j) < \varepsilon$, where ε is the proximity threshold.

The pseudo code of the Voronoi-based segmentation algorithm is given in algorithms 3.1 and the stages of the proposed method are depicted in figure 2.

Algorithm 1 Voronoi-based image segmentation algorithm

Input: Image I , Proximity Threshold ε

Output: Voronoi Segmented Image I_{seg}

```

function Voronoi_segmentation ( $I, \varepsilon$ )
2: Find N corners of  $I$ ,  $\{c_1, c_2, \dots, c_N\}$ 
   %Spatial Dirichlet tessellation
3: Find  $V = \{V_1, V_2, \dots, V_N\} : d(p, c_i) < d(p, c_j) \forall$  pixels  $p \in v_i, i \neq j$ 
   %Feature space Dirichlet tessellation
4: for each  $V_p \in V$  do
5:   Find set of feature vectors  $X_p = \{\overline{x}_1, \overline{x}_2, \dots, \overline{x}_m\}$  %  $\overline{x}_i =$  feature vector of
   pixel  $p_i \in V_p$ 
6:   Find the number of clusters  $k_p$ , cluster centroids  $C_p$  and set of clusters of  $X_p$ 
   using RSM module
7:    $X_p = \{s_1, s_2, \dots, s_{k_p}\}$ 
8: end for
   %Inter Voronoi region proximal cluster merging
9:  $S = \{s_1, s_2, \dots, s_P\} : S = \bigcup_{X_p} s_p \in X_p$ 
10:  $minProximity = \inf_{s_x, s_y \in S} (d(\overline{\mu}_x, \overline{\mu}_y))$ 
11: while  $minProximity < \varepsilon$  do
12:   Find the clusters  $s_i, s_j \in S$  that satisfy the merge condition and  $d(\overline{\mu}_i, \overline{\mu}_j) =$ 
    $\inf_{s_x, s_y \in S} (d(\overline{\mu}_x, \overline{\mu}_y))$ 
13:    $s_k = s_i \cup s_j$ 
14:   Find new cluster centroid
15:    $P = P - 1$ 
16:    $minProximity = \inf_{s_x, s_y \in S} (d(\overline{\mu}_x, \overline{\mu}_y))$ 
17: end while
18:  $I_{seg} = \{s'_1, s'_2, \dots, s'_M\}$ 
19: return  $I_{seg}$ 
20:end function

```

3.2. Analysis of the Computational Complexity. The main components, which contribute to the computational complexity of the AFHA algorithm are AS and FCM algorithms. The computational complexity of AS is $O(ncdi)$ and the computational complexity of FCM is $O(nc^2di)$ [12], where n is the number of data points, c is the number of clusters, d is the number of dimensions, i is the number of iterations. Thus, the computational complexity of AFHA algorithm can be given as $O(ncdi) + O(nc^2di)$. Similarly in the case of RFHA algorithm, the computational complexities of region splitting and merging phases are $O(n^r n^g n^b)$ and $O(idc^2)$ respectively and the complexity of the FCM algorithm is $O(nc^2di)$, where n^r, n^g and n^b are the number of valleys in the histograms of R,G and B channels respectively. Thus, the computational complexity of RFHA algorithm is $O(n^r n^g n^b) + O(idc^2) + O(nc^2di)$.

In the proposed algorithm, the regions splitting and merging happens within each Voronoï region leading to $O(\sum_{k=1}^N n_k^r n_k^g n_k^b)$ and $O(i_k d c_k^2)$ complexities in region splitting and merging stages respectively, where N is the number of Voronoï regions. It is important to note that the parameters n_k^r, n_k^g, n_k^b and c_k of the proposed method are much less compared to n^r, n^g, n^b and c of the RFHA algorithm as the region splitting and merging happen within small Voronoï regions in the proposed method rather than on the whole image as in RFHA. Also, the computational complexity of the K-means algorithm is $O(ncdi)$ [12], which is much less compared to the complexity of FCM $O(nc^2di)$. These factors contribute to lower the computational complexity of the proposed method. The computational complexity of the inter Voronoï region proximal cluster merging is $O(idc^2)$. Thus, the computational complexity of the proposed method is $O(\sum_{k=1}^N n_k^r n_k^g n_k^b + i_k d c_k^2) + O(idc^2) + O(ncdi)$.

The computational complexities of each algorithm reported in this article are summarized in table 1. Computational complexity of Mean-Shift algorithm is given as a reference.

Method	Computational Complexity
Mean-Shift	$O(n^2 di)$
AFHA	$O(ncdi) + O(nc^2 di)$
RFHA	$O(n^r n^g n^b) + O(idc^2) + O(nc^2 di)$
Proposed	$O(\sum_{k=1}^N n_k^r n_k^g n_k^b + i_k d c_k^2) + O(idc^2) + O(ncdi)$

TABLE 1. Comparison of computational complexity

n = number of data points, c = number of clusters, d = number of dimensions, i = number of iterations, N = number of Voronoï regions, n^r, n^g and n^b = number of valleys in the histograms of R,G and B channels respectively.

4. EXPERIMENTAL RESULTS AND ANALYSIS

The proposed algorithm was implemented in Matlab and its results were compared with the results of Matlab implementations of AFHA and RFHA algorithms. For the experiments, the latest version of the Berkeley Segmentation Dataset and Benchmark (BSDS500) [1, 20] was selected. Comparison of results of each algorithm for some sample images from BSDS500 data set is given in figures 3 and 4. During the implementation of the algorithm, ε is set to 71, which is said to be effective in detecting perceptually near clusters as given in [34].

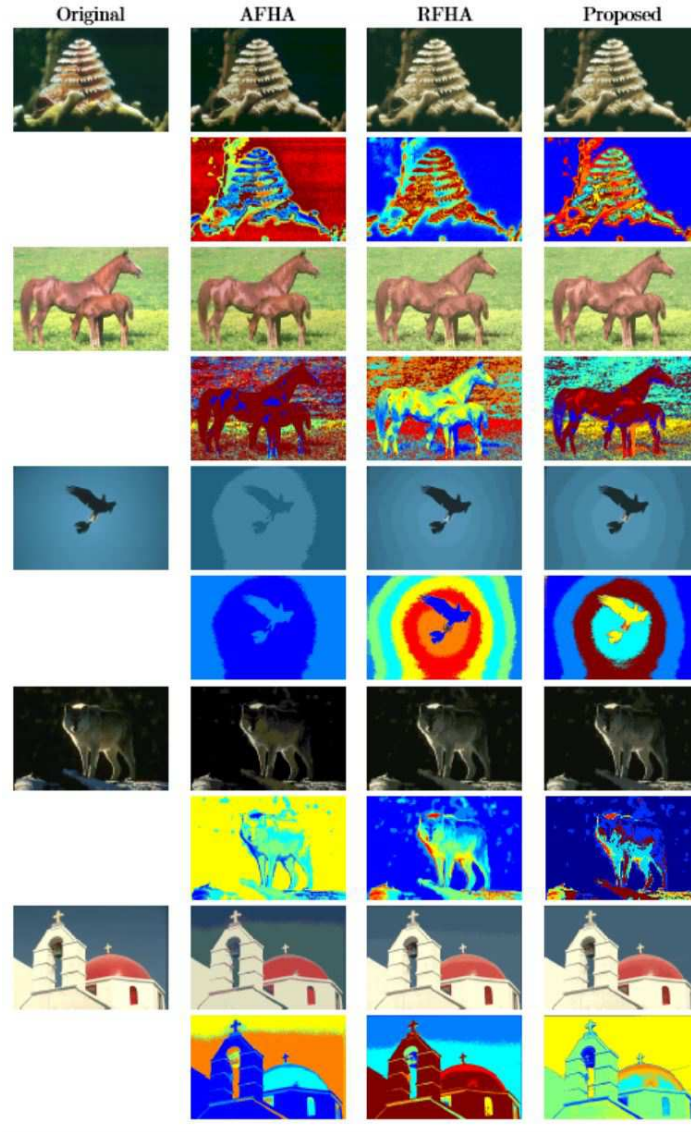


FIGURE 3. Comparison of results for sample images set 1 from BSD500 data set

4.1. Qualitative Analysis of the Segmentation Results. By observing figures 3 and 4, it is evident that the proposed method outperform the other two methods in terms of the segmentation results for the given sample images. For example, for the Coral image in figure 3, both AFHA and RFHA result in non-uniform background (so many isolated pixels in the background) while the proposed method preserves the homogeneity of the segment representing the background. This fact can be clearly seen by zooming in the segments given in false color (row 2 of Coral image results). Also, both AFHA and RFHA results in some misclassified pixels in the background and on the body of the horses in the Horses image. For the Bird image,

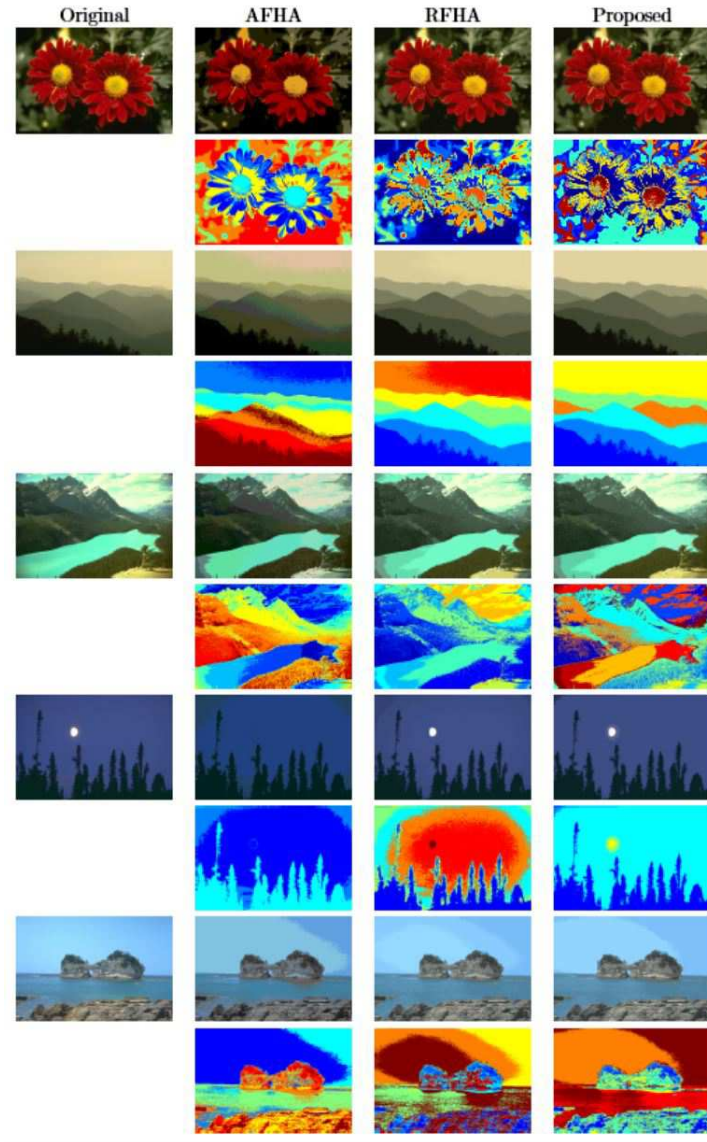


FIGURE 4. Comparison of results for sample images set 2 from BSD500 data set

AFHA fails to give a satisfactory segmentation (centroid colors are far deviated from the original colors) while RFHA produces a segmented image with too many segments in the region of the sky. The proposed method provides a satisfactory segmentation for both these images.

AFHA fails to provide a satisfactory segmentation for the Wolf image as some of the pixels on the Wolf's body are misclassified. The result of RFHA and the proposed method are almost the same except for the fact that RFHA segmented image has more noise in the background. The segmentation result of the proposed

method and the RFHA algorithm is very much alike for the River image and Flowers image given in figure 4. However, the segmentation of the tree line at the bottom right hand side of the River image segmented by the proposed method is clearer compared to the RFHA segmented image. Furthermore, the proposed method provides the best segmentation result for the Moon image. Both AFHA and RFHA results in over-segmentation of the sky area and AFHA fails to segment the moon in the Moon image.

Similarly, both AFHA and RFHA results in over-segmentation of the sky region in the Church image and Mountains image and RFHA results in over-segmentation of the sky region in the Sea image. Also, AFHA results in misclassified pixels in the segmented Mountains, Church and Sea images. The proposed method provides a more uniform segmentation results for all three images.

By observing the results given in figures 3 and 4, it is evident that the proposed method is more robust in segmenting large homogenous regions such as the sky region in all sample images. Segmentation results of AFHA commonly shows misclassified pixels and segments having centroid colors much deviated from the original colors and the segmentation results of RFHA are mostly over-segmented. These facts become evident, when comparing the segmentation results given in false color in figures 3 and 4.

Furthermore, the segmentation results of the proposed method can be further improved by varying the predefined threshold ε depending on the application. For example, figure 5 depicts how the segmentation result of the sample image 2 can be improved by increasing the ε from 71 to 150. It is important to note that similar change of the predefined threshold (dc) in RFHA does not result in such improved segmentation, when the predefined threshold is increased to 150. RFHA results in an under-segmented image for $dc = 150$.

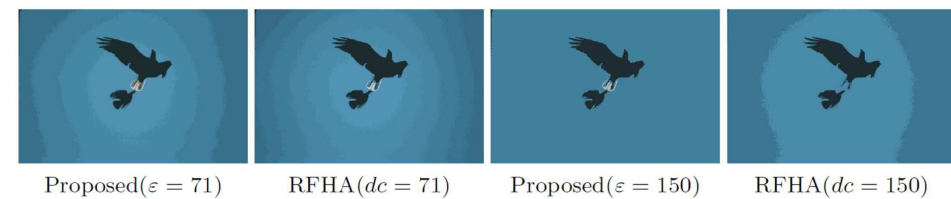


FIGURE 5. Comparison of results for variations of ε

4.2. Quantitative Analysis of the Segmentation Results. There are multiple benchmarks reported in the past literature to evaluate the image segmentation results. Zhang et al. [39] broadly categorizes these evaluation methods into supervised evaluation methods, which evaluates segmentation algorithms by comparing the resulting segmented image against a manually segmented reference image or ground truth and unsupervised evaluation methods, which evaluate a segmented image based on how well it matches a broad set of characteristics of segmented images as desired by humans. Supervised evaluation is subjective and time consuming while the unsupervised evaluation is quantitative and objective. In this article, we will be using the unsupervised evaluation methods.

We first started with the *Mean Squared Error (MSE)*, which is one of the most fundamental benchmark used to evaluate cluster quality. MSE can be calculated

by using the equation (3). The number of clusters and cluster quality for the four sample images given in figures 3 and 4 are reported in table 2.

$$(3) \quad MSE = \frac{1}{N} \sum_{j=1}^M \sum_{i \in S_j} \|x_i - c_j\|^2$$

where N is the total number of pixels in the images, M is the number of clusters produced during the clustering process, S_j is the set of pixels belonging to j^{th} cluster, c_j is the feature vector of the j^{th} cluster centroid and x_i is the feature vector of the i^{th} pixel belonging to j^{th} cluster. Thus, MSE measure the average deviation of the pixels from the cluster centroids.

Image	No. of Clusters			MSE (*1.0e+3)		
	AFHA	RFHA	Proposed	AFHA	RFHA	Proposed
Coral	9	10	9	1.1727	0.2886	0.2964
Horses	23	8	13	1.0874	0.6335	0.3755
Bird	2	8	8	1.3135	0.0479	0.0561
Wolf	5	7	7	0.8897	0.1760	0.1704
Church	6	11	12	1.6880	0.1567	0.1862
Flowers	7	15	18	1.9896	0.2946	0.2372
Mountains	12	7	6	1.0085	0.0943	0.1156
River	16	11	16	1.2827	0.4535	0.2911
Moon	3	8	5	1.2717	0.0413	0.0970
Sea	8	11	10	1.4449	0.2283	0.2374

TABLE 2. Comparison of no. of clusters and MSE of different algorithms

The results given in table 2 shows that the proposed method results in a very low MSE for all the sample images. For all the sample images, AFHA results in the highest MSE for all sample images. RFHA results in the lowest MSE for six images namely, Coral, Bird, Church, Mountains, Moon and Sea and the proposed method results in the lowest MSE for four images namely, Horses, Wolf, Flowers and River. Overall, for the 200 images that was used in the experiments, the proposed method results in 47% of the images with the lowest MSE and RFHA results in 53% of the images with the lowest MSE. Thus, with respect to MSE alone, RFHA seems to perform better than the proposed method.

However, MSE alone has not proven to be a very reliable benchmark for the evaluation of image segmentation results. There is always a trade-off between preserving details and suppressing noise. If there are too many segments in the segmented image, then the difference between pixels belonging to a cluster and the cluster centroid may be lower leading to a smaller MSE. But, since many small clusters are formed and the number of clusters is large, the segmented image may not be a satisfactory one. Therefore, further analysis with regard to the number of clusters and homogeneity of clusters is essential for successful evaluation of the proposed segmentation algorithm.

Liu and Yang proposed an image segmentation evaluation function $F(I)$ in [18], which penalizes the over-segmentation in segmented images. $F(I)$ can be calculated by using equation (4).

$$(4) \quad F(I) = \frac{\sqrt{M}}{1000 \times N} \sum_{j=1}^M \frac{e_j^2}{\sqrt{N_j}}$$

where I is the image to be segmented, M is the number of segments in the segmented image, N_j is the number of pixels in the j^{th} segment and e_j is the color error of region j . e_j is defined as the sum of the Euclidean distances of the feature vectors between the original image and the segmented image of each pixel region.

The term \sqrt{M} in $F(I)$ penalizes the segmentation which form too many segments. e_j indicates whether or not a region is assigned an appropriate feature (color). If the resulting image is over-segmented, the color error of each segment may be smaller, but since the number of segments is large, the value of F will be large indicating that the segmentation result is not good. On the other hand, if the resulting image is under-segmented, then the number of segments will be reduced, but the color error of each segment will be large leading to a large F .

A modified version of $F(I)$ named $F'(I)$ was proposed by Borsotti et al. in [3]. Borsotti et al. propose to modify the global penalization measure \sqrt{M} used in $F(I)$ to make it more robust for noisy images. Borsotti et al. also proposed another evaluation function named $Q(I)$ in [3], which is said to be more sensitive to small segmentation differences. $Q(I)$ uses a stronger penalization factor to penalize non-homogeneous regions. The equations to calculate $F'(I)$ and $Q(I)$ are given in equations (5) and (6).

$$(5) \quad F'(I) = \frac{\sum_{j=1}^M e_j^2 \sqrt{\sum_{a=1}^{MaxArea} [S(a)]^{1+(1/a)}}}{(1000 \times N) \sqrt{N_j}}$$

$$(6) \quad Q(I) = \frac{1}{1000 \times N} \sqrt{M} \sum_{j=1}^M \left[\frac{e_j^2}{1 + \log N_j} + \left(\frac{S(N_j)}{N_j} \right)^2 \right]$$

where N is the total number of pixels in image I , M is the number of segments, N_j is the number of pixels in j^{th} segment, $S(a)$ denotes the number of regions in image I that has an area of exactly a and $MaxArea$ denotes the largest region in the segmented image.

Thus, next $F(I)$, $F'(I)$ and $Q(I)$ were measured in order to perform a more comprehensive evaluation of the proposed method. Since, the number of small segments in the segmented images produced by the algorithms reported in this article was very much low, the experimental results for $F(I)$ and $F'(I)$ were the same. As the number of small regions reduces, $\sqrt{\sum_{a=1}^{MaxArea} [S(a)]^{1+(1/a)}}$ approximates to \sqrt{M} . Therefore, only the values of $F'(I)$ and $Q(I)$ will be reported in this section. Table 3 provides a comparison of the results for $F'(I)$ and $Q(I)$ evaluation functions for different algorithms.

By observing the results given in table 3, it is evident that the proposed method results in the lowest $F'(I)$ and $Q(I)$ for majority of the sample images. The results of $F'(I)$ and $Q(I)$ are consistent for all sample images. The proposed methods results in the lowest $F'(I)$ and $Q(I)$ for Coral, Horses, Wolf, Flowers, River and Sea images while RFHA results in the lowest $F'(I)$ and $Q(I)$ for Bird, Church, Mountains and Moon images. It is important note that the proposed method had

Image	$F'(I)$			$Q(I)$		
	AFHA	RFHA	Proposed	AFHA	RFHA	Proposed
Coral	0.0280	0.0101	0.0093	0.3329	0.0891	0.0875
Horses	0.0628	0.0136	0.0135	0.5503	0.1657	0.1332
Bird	0.0067	0.0016	0.0020	0.1514	0.0144	0.0200
Wolf	0.0140	0.0052	0.0048	0.1775	0.0454	0.0443
Church	0.0246	0.0065	0.0067	0.3926	0.0532	0.0668
Flowers	0.0370	0.0148	0.0142	0.4788	0.1124	0.1077
Mountains	0.0276	0.0017	0.0018	0.3730	0.0229	0.0256
River	0.0537	0.0143	0.0131	0.5149	0.1442	0.1175
Moon	0.0086	0.0011	0.0015	0.1982	0.0113	0.0246
Sea	0.0274	0.0072	0.0071	0.3988	0.0726	0.0721

TABLE 3. Comparison of $F'(I)$ and $Q(I)$ evaluation functions of different algorithms

higher MSE compared to RFHA for Coral and Sea images, but the $F'(I)$ and $Q(I)$ values for the same images are lower compared to the RFHA method. This is due to the penalization of over-segmentation available in $F'(I)$ and $Q(I)$. AFHA results in the highest values for $F'(I)$ and $Q(I)$ for all the sample images. Overall, the proposed method results in the lowest $F'(I)$ and $Q(I)$ for 63% of the 200 images used in experiments. RFHA results in the lowest $F'(I)$ and $Q(I)$ for only 37% of the 200 images in the data set.

The image segmentation evaluation functions F proposed in [18] and F' and Q proposed in [3] fall under the first evaluation criteria given in [13], which measure the intra-cluster uniformity. It is said in [39] that F , F' and Q are biased towards under-segmentation because they use a weighting factor to penalize against over-segmentation. Also, F , F' and Q do not measure the inter-region disparity (the second criteria in [13]), which is vital for fair evaluation of segmentation results.

Thus, next we use the evaluation function F_{RC} proposed by Rosenberger and Chehdi in [29] to cover both evaluation criteria. F_{RC} has two evaluation functions to measure both the intra-region uniformity and inter-region disparity. The first function $\underline{D}(I^j)$ measures the global intra-region uniformity, which quantifies the homogeneity of each region in the segmented image I^j and the second function $\overline{D}(I^j)$ measures the global inter-region disparity between regions.

$$(7) \quad \underline{D}(I^j) = \frac{1}{M} \sum_{j=1}^M \frac{N_j}{N} \underline{D}(R_j)$$

$$(8) \quad \overline{D}(I^j) = \frac{1}{M} \sum_{j=1}^M \frac{N_j}{N} \overline{D}(R_j)$$

M is the number of segments, N_j is the number of pixels in j^{th} segment R_j , N is the total number of pixels in image I_j . According to [39], the $\underline{D}(R_j)$ in the case of color images is computed as the average squared color error of region R_j . The inter-region disparity between two regions is calculated as:

$$(9) \quad D(R_i, R_j) = \frac{|E(R_i) - E(R_j)|}{NG}$$

where $E(R_i)$ is the average gray-level in the region R_i and NG is the number of gray levels in the image. In the case color images, we will be using the average color difference between the cluster centers to measure $D(R_i, R_j)$.

The intra-region and inter-region metrics were combined in order to find the F_{RC} in [29] as follows.

$$(10) \quad F_{RC} = F(\underline{D}(I^j), \overline{D}(I^j)) = \frac{\overline{D}(I^j) - \underline{D}(I^j)}{2}$$

Image	$\underline{D}(I^j)$			$\overline{D}(I^j)$			F_{RC}		
	AFHA	RFHA	Proposed	AFHA	RFHA	Proposed	AFHA	RFHA	Proposed
Coral	19.3304	2.2217	3.9567	28.0100	28.0764	32.7834	4.3398	12.9273	14.4133
Horses	2.6996	9.5929	2.3926	6.2871	19.1335	12.0146	1.7938	4.7703	4.8110
Bird	323.2662	0.6789	1.3421	48.0000	14.0926	16.4910	-137.6331	6.7069	7.5744
Wolf	66.8444	2.6871	3.6571	50.9932	36.4489	39.0588	-7.9256	16.8809	17.7008
Church	72.7586	1.4397	3.8182	40.7715	23.9536	21.5476	-15.9936	11.2569	8.8647
Flowers	43.7067	1.2160	0.8677	24.7662	12.3263	11.9862	-9.4702	5.5515	5.55925
Mountains	11.0262	1.8963	3.6470	19.4786	37.0116	43.2205	4.2262	17.5576	19.7868
River	5.2477	3.5570	1.2531	15.3580	21.6964	18.7902	5.0552	9.0697	8.76855
Moon	218.7566	0.8104	8.5069	35.4797	20.7144	45.2829	-91.6385	9.9520	18.3880
Sea	37.7216	1.8485	2.5008	23.8559	17.4988	19.6872	-6.9329	7.8252	8.5932

TABLE 4. Comparison of $\underline{D}(I^j)$, $\overline{D}(I^j)$ and F_{RC} evaluation functions of different algorithms

A comparison of the values for $\underline{D}(I^j)$, $\overline{D}(I^j)$ and F_{RC} evaluation functions of the proposed method and AFHA and RFHA algorithms is given in table 4. It is said in [39] that F_{RC} is more balanced with respect to under-segmentation and over-segmentation with only slight or negligible biases one way or the other. This fact becomes evident by observing the results given in table 4. In the results given in 4, RFHA produces the lowest intra-region uniformity for majority of the sample images and AFHA produces the highest inter-region disparity for the majority of the sample images. However, it is important to note that the proposed method produces the best values for the combined metric F_{RC} for majority of the sample images, which means the proposed method produced a balanced result that preserves both the intra-region uniformity and inter-region disparity at the same time.

Overall, the proposed method results in the best F_{RC} for 71% of the 200 images used in experiments. RFHA results in the best F_{RC} for 29% of the 200 images in the data set while AFHA results in the worst F_{RC} for all 200 images. Thus, we can conclude that the proposed method outperforms both AFHA and RFHA in terms of the image segmentation quality.

4.3. Analysis of the Execution Time. Some experiments were conducted in order to compare the execution times of the proposed method with AFHA and RFHA. Table 5 shows the execution time of each algorithm run on a Intel Xeon E3-1280 V2 @ 3.60 GHz processor for the 10 sample images reported in the experiments section. Also, the average execution time per image of each algorithm was measured by segmenting the 200 training images in the BSDS500 data set. The results are given in table 6.

Image	Image Size	Execution Time (seconds)		
		AFHA	RFHA	Proposed
Coral	481 × 321	38.1181	509.9087	30.0898
Horses	481 × 321	60.8689	14.7592	32.8365
Bird	481 × 321	31.1224	47.4568	3.7746
Wolf	481 × 321	37.9469	64.9920	11.6247
Church	481 × 321	35.5790	27.9902	9.6971
Flowers	481 × 321	45.5225	92.5119	21.3567
Mountains	481 × 321	39.5727	6.1321	7.1426
River	481 × 321	73.1063	40.8520	20.6950
Moon	481 × 321	28.7676	58.6831	9.2689
Sea	481 × 321	46.7545	27.3802	21.9857

TABLE 5. Comparison of execution times of different algorithms for sample images

Method	Avg. Execution Time (seconds)
AFHA	65.3978
RFHA	52.3573
Proposed	21.8905

TABLE 6. Comparison of average execution time per image for 200 images of BSDS500 data set

By observing the results given in tables 5 and 6, we can conclude that the proposed method outperforms AFHA and RFHA in terms of the computational complexity. The average execution time per image of the proposed method is roughly 22 seconds, which is the lowest compared to the other two methods. The average execution time per image of the AFHA method is roughly 65 seconds, which is the highest and the average execution time of the RFHA method is roughly 52 seconds. Thus, the average execution time per image of the proposed method is improved by 57.69% compared to the RFHA method. Thus, the proposed method is proven to be more suitable for real-time image segmentation applications.

5. CONCLUSION

In this article, a new adaptive unsupervised algorithm based on Voronoï regions was proposed to solve the image segmentation problem. The proposed algorithm is capable of automatically determining the number of clusters and the cluster centroids in a given set of pixels. The proposed algorithm adaptively divides the image into Voronoï regions and performs region splitting and merging within Voronoï regions to find intra-Voronoï region clusters, which will then be iteratively merged to find the final number of clusters and cluster centroids. In contrast to existing algorithms, K-means clustering algorithm is used to find the final segmented image in the proposed method in place of the FCM algorithm. The Voronoï region wise clustering in the proposed algorithm leads to significant reduction in the computational complexity of the image segmentation problem. Furthermore, since the number of possible clusters within a single Voronoï region is usually lower compared

to the number of clusters in the whole image, estimating the number of clusters and cluster centroids becomes more efficient and precise.

The experimental results reported in this article confirm that the proposed method outperforms two other adaptive unsupervised cluster-based image segmentation algorithms, AFHA and RFHA in terms of the image segmentation quality based on three different unsupervised image segmentation evaluation benchmarks. Also, the results of the experiments on average execution time per image prove that the proposed method is much faster compared to the other two algorithms reported in this article, which makes the proposed method more suitable for real-time image segmentation applications.

REFERENCES

1. *The Berkeley Segmentation Dataset and Benchmark*, 2007, <https://www.eecs.berkeley.edu/Research/Projects/CS/vision/bsds/>.
2. Kishore Bhojar and Omprakash Kakde, *Color image segmentation based on jnd color histogram*, International Journal of Image Processing (IJIP) **3** (2010), no. 6, 283.
3. M Borsotti, Paola Campadelli, and Raimondo Schettini, *Quantitative evaluation of color image segmentation results*, Pattern recognition letters **19** (1998), no. 8, 741–747.
4. Robert L Cannon, Jitendra V Dave, and James C Bezdek, *Efficient implementation of the fuzzy c-means clustering algorithms*, Pattern Analysis and Machine Intelligence, IEEE Transactions on (1986), no. 2, 248–255.
5. Abbas Cheddad, Joan Condell, Kevin Curran, and Paul Mc Kevitt, *On points geometry for fast digital image segmentation*, The 8th International Conference on Information Technology and Telecommunication. Ireland: IEEE, 2008, pp. 54–61.
6. Heng-Da Cheng, XH Jiang, Ying Sun, and Jingli Wang, *Color image segmentation: advances and prospects*, Pattern recognition **34** (2001), no. 12, 2259–2281.
7. Alberto Coloni, Marco Dorigo, Vittorio Maniezzo, et al., *Distributed optimization by ant colonies*, Proceedings of the first European conference on artificial life, vol. 142, Paris, France, 1991, pp. 134–142.
8. G.L. Dirichlet, *Über die reuktion der positiven quadratischen formen mit drei unbestimmten ganzen zahlen*, J. für die reine und angewandte Math. **40** (1850), 209–227.
9. Qiang Du, Vance Faber, and Max Gunzburger, *Centroidal voronoi tessellations: applications and algorithms*, SIAM review **41** (1999), no. 4, 637–676.
10. Qiang Du, Max Gunzburger, Lili Ju, and Xiaoqiang Wang, *Centroidal voronoi tessellation algorithms for image compression, segmentation, and multichannel restoration*, Journal of Mathematical Imaging and Vision **24** (2006), no. 2, 177–194.
11. Keinosuke Fukunaga and Larry D Hostetler, *The estimation of the gradient of a density function, with applications in pattern recognition*, Information Theory, IEEE Transactions on **21** (1975), no. 1, 32–40.
12. Soumi Ghosh and Sanjay Kumar Dubey, *Comparative analysis of k-means and fuzzy c-means algorithms*, International Journal of Advanced Computer Science and Applications **4** (2013), no. 4, 34–39.
13. Robert M Haralick and Linda G Shapiro, *Image segmentation techniques*, Computer vision, graphics, and image processing **29** (1985), no. 1, 100–132.
14. John A Hartigan and Manchek A Wong, *Algorithm as 136: A k-means clustering algorithm*, Journal of the Royal Statistical Society. Series C (Applied Statistics) **28** (1979), no. 1, 100–108.
15. Dana E Ilea and Paul F Whelan, *Ctexas adaptive unsupervised segmentation algorithm based on color-texture coherence*, Image Processing, IEEE Transactions on **17** (2008), no. 10, 1926–1939.
16. Anil K Jain and Richard C Dubes, *Algorithms for clustering data*, Prentice Hall, Inc., 1998.
17. W ladys law Skarbek and Andreas Koschan, *Colour image segmentation a survey*, IEEE Transactions on circuits and systems for Video Technology **14** (1994), no. 7.
18. Jianqing Liu and Yee-Hong Yang, *Multiresolution color image segmentation*, Pattern Analysis and Machine Intelligence, IEEE Transactions on **16** (1994), no. 7, 689–700.

19. Stuart Lloyd, *Least squares quantization in pcm*, IEEE Transactions on Information Theory **28** (1982), no. 2, 129–137.
20. D. Martin, C. Fowlkes, D. Tal, and J. Malik, *A database of human segmented natural images and its application to evaluating segmentation algorithms and measuring ecological statistics*, Proc. 8th Int'l Conf. Computer Vision, vol. 2, July 2001, pp. 416–423.
21. Marija J Norušis, *Ibm spss statistics 19 statistical procedures companion*, Prentice Hall, 2012.
22. Rafail Ostrovsky, Yuval Rabani, Leonard J Schulman, and Chaitanya Swamy, *The effectiveness of lloyd-type methods for the k-means problem*, Foundations of Computer Science, 2006. FOCS'06. 47th Annual IEEE Symposium on, IEEE, 2006, pp. 165–176.
23. Nikhil R Pal and Sankar K Pal, *A review on image segmentation techniques*, Pattern recognition **26** (1993), no. 9, 1277–1294.
24. Dan Pelleg, Andrew W Moore, et al., *X-means: Extending k-means with efficient estimation of the number of clusters.*, ICML, vol. 1, 2000.
25. J.F. Peters, *Topology of digital images. Visual pattern discovery in proximity spaces*, Intelligent Systems Reference Library **63** (2014), xv + 411pp, DOI: 10.1007/978-3-642-53845-2, Zentralblatt MATH Zbl 1295 68010.
26. ———, *Computational proximity. Excursions in the topology of digital images.*, Intelligent Systems Reference Library **102** (2016), xxvi + 433pp, DOI: 10.1007/978-3-319-30262-1, in press.
27. J.F. Peters and E. İnan, *Strongly near Voronoi nucleus clusters*, arXiv **1602** (2016), no. 03734, 1–7.
28. Charles Romesburg, *Cluster analysis for researchers*, Lulu Press, 2004.
29. Christophe Rosenberger and Kacem Chehdi, *Genetic fusion: application to multi-components image segmentation*, Acoustics, Speech, and Signal Processing, 2000. ICASSP'00. Proceedings. 2000 IEEE International Conference on, vol. 6, IEEE, 2000, pp. 2223–2226.
30. ———, *Unsupervised clustering method with optimal estimation of the number of clusters: Application to image segmentation*, Pattern Recognition, 2000. Proceedings. 15th International Conference on, vol. 1, IEEE, 2000, pp. 656–659.
31. Jianbo Shi and Jitendra Malik, *Normalized cuts and image segmentation*, Pattern Analysis and Machine Intelligence, IEEE Transactions on **22** (2000), no. 8, 888–905.
32. MA Suhail, MS Obaidat, SS Ipson, and B Sadoun, *Content-based image segmentation*, Systems, Man and Cybernetics, 2002 IEEE International Conference on, vol. 5, IEEE, 2002, pp. 6–pp.
33. M Sujaritha and S Annadurai, *Color image segmentation using adaptive spatial gaussian mixture model*, International journal of signal processing **6** (2010), no. 1, 28–32.
34. Khang Siang Tan, Nor Ashidi Mat Isa, and Wei Hong Lim, *Color image segmentation using adaptive unsupervised clustering approach*, Applied Soft Computing **13** (2013), no. 4, 2017–2036.
35. Luis Garcia Ugarriza, Eli Saber, Sreenath Rao Vantaram, Vincent Amuso, Mark Shaw, and Ranjit Bhaskar, *Automatic image segmentation by dynamic region growth and multiresolution merging*, Image Processing, IEEE Transactions on **18** (2009), no. 10, 2275–2288.
36. Sreenath Rao Vantaram and Eli Saber, *An adaptive bayesian clustering and multivariate region merging based technique for efficient segmentation of color images*, Acoustics, Speech and Signal Processing (ICASSP), 2011 IEEE International Conference on, IEEE, 2011, pp. 1077–1080.
37. G. Voronoi, *Nouvelles applications des paramètres continus à la théorie des formes quadratiques*, J. für die reine und angewandte Math. **133** (1907), 97–178.
38. Zhiding Yu, Oscar C Au, Ruobing Zou, Weiyu Yu, and Jing Tian, *An adaptive unsupervised approach toward pixel clustering and color image segmentation*, Pattern Recognition **43** (2010), no. 5, 1889–1906.
39. Hui Zhang, Jason E Fritts, and Sally A Goldman, *Image segmentation evaluation: A survey of unsupervised methods*, computer vision and image understanding **110** (2008), no. 2, 260–280.

^{α} COMPUTATIONAL INTELLIGENCE LABORATORY, UNIVERSITY OF MANITOBA, WPG, MB, R3T 5V6, CANADA

^{β} DEPARTMENT OF MATHEMATICS, FACULTY OF ARTS AND SCIENCES, ADIYAMAN UNIVERSITY, 02040 ADIYAMAN, TURKEY